Quarkyonic matter and quarkyonic stars in an extended relativistic mean field model

Cheng-Jun Xia[1,*] Hao-Miao Jin,[1,2] and Ting-Ting Sun[2]

[1]*Center for Gravitation and Cosmology, College of Physical Science and Technology,*
Yangzhou University, Yangzhou 225009, China
[2]*School of Physics and Microelectronics, Zhengzhou University, Zhengzhou 450001, China*

By combining relativistic mean field models and equivparticle models with density-dependent quark masses, we construct explicitly "a quark Fermi sea" and "a baryonic Fermi surface" to model the quarkyonic phase, where baryons with momentums ranging from zero to Fermi momentums are included. The properties of nuclear matter, quark matter, and quarkyonic matter are then investigated in a unified manner, where quarkyonic matter is more stable and energy minimization is still applicable to obtain the microscopic properties of dense matter. Three different covariant density functionals TW99, PKDD, and DD-ME2 are adopted in our work, where TW99 gives satisfactory predictions for the properties of nuclear matter in both neutron stars and heavy-ion collisions and quarkyonic transition is unfavorable. Nevertheless, if PKDD with larger slope of symmetry energy L or DD-ME2 with larger skewness coefficient J are adopted, the corresponding equations of state (EOSs) are too stiff according to both experimental and astrophysical constraints. The situation is improved if quarkyonic transition takes place, where the EOSs become softer and can accommodate various experimental and astrophysical constraints.

I. INTRODUCTION

Because of the asymptotic freedom and confinement of strong interactions at large and small energy scales, the strongly interacting matter at zero temperature is believed to exhibit at least two phases, i.e., low-density hadronic matter (HM) and high-density quark matter (QM). As density increases, HM may undergo a deconfinement phase transition and form QM, while it is not clear what exactly happens in the processes of deconfinement phase transition and many possibilities exist [1,2]. For example, one type of deconfinement phase transitions from HM to QM are of first order [3], indicating the possible existence of a quark-hadron mixed phase inside hybrid stars [4–15]. The other type of deconfinement phase transitions resemble those at vanishing chemical potentials and large temperatures, where a smooth crossover between HM and quark-gluon plasma takes place [16,17]. The hadron-quark crossover at finite densities was modeled with various phenomenological interpolation functions, which predicts a stiffer equation of state (EOS) so that a hybrid star could reach $2M_{\odot}$ [18–31]. The implications of such a hadron-quark crossover on binary neutron

star mergers and the postmerger gravitational signals were then examined, which could be identified by future kilohertz gravitational wave detectors [32,33].

To unveil the microscopic dynamics for the crossover domain, as demonstrated by Fukushima and Kojo [34], the crossover from HM to QM can be bridged by quarkyonic matter. At supranuclear densities, the many-body interactions between baryons become significant [35], which is attributed to the increasing number of exchanged quarks [34]. The boundary between baryons eventually becomes blurred and quarks can move freely among baryons at large densities, i.e., forming the quarkyonic phase [36]. As proposed by McLerran and Pisarski in the large N_c limit [37], a quarkyonic phase is comprised of "a quark Fermi sea" and "a baryonic Fermi surface." Further studies on the phase diagram of strongly interacting matter with an extended Nambu-Jona-Lasinio model suggest that the quarkyonic transition is indeed a crossover at $N_c = 3$ [38]. It was shown that the pressure and sound velocity of quarkyonic matter increase rapidly with density, which fulfills the observational constraints on massive neutron stars [39]. The effects of isospin-flavor asymmetry was later considered, predicting a lower proton fraction which could potentially quench fast cooling in massive quarkyonic stars [40]. By synthesizing the Walecka model together with the quark-meson model, a complete field model for quarkyonic matter treating baryons, quarks, and mesons on the same footing was developed [41,42], where the chiral symmetry breaking and restoration in quarkyonic

*cjxia@yzu.edu.cn

matter can be described. In the framework of a constituent quark model, the emergence of quarkyonic modes in dense baryonic matter was analyzed as well, where the attractive *ud* color antitriplet diquark remains intact [43,44].

For baryonic matter below and around the nuclear saturation density n_0, relativistic mean field (RMF) models are often adopted [45], which give an excellent description for finite nuclei [46–56] and nuclear matter [57–65]. In such cases, it is natural to extend RMF models to include quark degrees of freedom, which was done by combining RMF models and equivparticle models with density-dependent quark masses [66]. In this work, based on our previous study [66], we construct explicitly a quark Fermi sea and a baryonic Fermi surface to model the quarkyonic phase. A schematic illustration of the corresponding quarkyonic phase is presented in Fig. 1, where the Fermi distributions of quarks from the quark Fermi sea and baryonic Fermi surface are indicated by the red and cyan regions, respectively. The single-particle energies of quarks (ϵ_q, red dashed curve) and baryons (ϵ_b, black solid curve) as functions of their momentums p_q and p_b are presented, which are matched at $p_b = 0$ and $\epsilon_b = 3\epsilon_q \neq 0$ as denoted by the horizontal line. It is worth mentioning that, in contrast to previous constructions of the Fermi sphere for quarkyonic matter by simply removing lower-momentum components [39–42], baryons with momentums ranging from zero to Fermi momentums are considered here. We believe such treatment is more natural, since the low-energy excitations should carry vanishing momentums
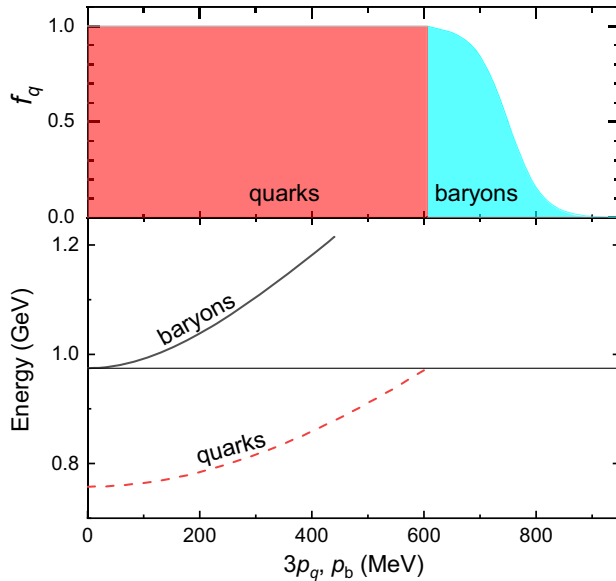
FIG. 1. Schematic plot on the occupation function f_q for quarks with momenta p_q in the quarkyonic phase, which is comprised of two parts, i.e., those from the quark Fermi sea (red area) and baryonic Fermi surface (cyan area). The corresponding dispersion relations of quarks ($3\epsilon_q$-$3p_q$) and nucleons (ϵ_b-p_b) are indicated in the lower panel as well.

analogous to the formation of Cooper pairs [67], which is dominated by zero-momentum components. The quarks confined within baryons can be viewed as wave packets, and we expect a widespread momentum distribution for quarks in the baryonic Fermi surface. Despite the small total momentum of three quarks forming a baryon, a lower-momentum cutoff exists due to the effects of Pauli blocking from the quark Fermi sea, which alters the masses of baryons and results in the peculiar momentum distribution as illustrated by the cyan area in Fig. 1.

The interactions between baryons are treated with the RMF approach via exchange of σ, ω, and ρ mesons, where the baryon-meson couplings are density dependent, adopting the effective interactions TW99 [51], PKDD [68], and DD-ME2 [69]. The quarks are considered as quasifree particles with density-dependent masses, including confinement and leading-order perturbative interactions [70]. Finally, the quark-baryon interactions are accounted for with density-dependent baryon masses, and energy minimization is still applicable to obtain microscopic properties of quarkyonic matter. The paper is organized as follows. In Sec. II, we present the theoretical framework for nuclear matter, quark matter, and quarkyonic matter. The properties of dense matter and the implication for compact star structures are then examined in Sec. III. We draw our conclusion in Sec. IV.

II. THEORETICAL FRAMEWORK

The Lagrangian density of the extended RMF model can be divided into the following three parts:

$$\mathcal{L} = \mathcal{L}^{\text{B}} + \mathcal{L}^{\text{Q}} + \mathcal{L}^{\text{L}}, \tag{1}$$

where $\mathcal{L}^{\text{B}}$, $\mathcal{L}^{\text{Q}}$, and $\mathcal{L}^{\text{L}}$ are, respectively, the Lagrangian densities for nuclear matter, quark matter, and leptonic matter, i.e.,

$$\mathcal{L}^{\text{B}} = \sum_{i=n,p} \bar{\Psi}_i \{ i\gamma^\mu \partial_\mu - m_i(n_{\text{b}}^{\text{Q}}) - g_{\sigma i}(n_{\text{b}}^{\text{B}})\sigma$$
$$- g_{\omega i}(n_{\text{b}}^{\text{B}})\gamma^\mu \omega_\mu - g_{\rho i}(n_{\text{b}}^{\text{B}})\gamma^\mu \boldsymbol{\tau}_i \cdot \boldsymbol{\rho}_\mu \} \Psi_i$$
$$- \frac{1}{2}m_\sigma^2\sigma^2 + \frac{1}{2}m_\omega^2\omega_\mu\omega^\mu + \frac{1}{2}m_\rho^2\boldsymbol{\rho}_\mu \cdot \boldsymbol{\rho}^\mu, \tag{2}$$

$$\mathcal{L}^{\text{Q}} = \sum_{i=u,d} \bar{\Psi}_i [i\gamma^\mu \partial_\mu - m_i(n_{\text{b}})]\Psi_i, \tag{3}$$

$$\mathcal{L}^{\text{L}} = \sum_{i=e,\mu} \bar{\Psi}_i [i\gamma^\mu \partial_\mu - m_i]\Psi_i. \tag{4}$$

Here Ψ_i represents the Dirac spinor for different fermions i (baryons, quarks, and leptons) with masses m_i, where $m_{n,p}(n_{\text{b}}^{\text{Q}})$ and $m_{u,d}(n_{\text{b}})$ are density dependent with n_{b}^{B}, n_{b}^{Q}, and n_{b} being, respectively, the baryon number densities for nucleons, quarks, and both particles combined, i.e.,

$$n_b^B = n_p + n_n; \quad n_b^Q = (n_u + n_d)/3; \quad n_b = n_b^B + n_b^Q. \quad (5)$$

The isospin of baryons is denoted by τ_i. To describe the baryon-baryon interactions, the isoscalar-scalar meson σ, isoscalar-vector meson ω_μ, and isovector-vector meson ρ_μ are introduced with $m_\sigma(g_{\sigma i})$, $m_\omega(g_{\omega i})$, and $m_\rho(g_{\rho i})$ being their masses (coupling constants), respectively. For a system with time-reversal symmetry, the spacelike components of the vector fields ω_μ and ρ_μ vanish, leaving only the time components ω_0 and ρ_0. Meanwhile, charge conservation guarantees that only the third component $\rho_{0,3}$ in the isospin space survives. Note that, for uniform dense matter σ, ω_0, and $\rho_{0,3}$ are independent of the space coordinates, so that their space and time derivatives vanish.

In the quarkyonic phase, baryons and quarks coexist inside the same volume. Similar to the treatments of α clustering inside nuclear matter in Refs. [71,72], we adopt a phenomenological baryon mass scaling to consider the effects of Pauli blocking and interactions between quarks and baryons, i.e.,

$$m_i(n_b^Q) = m_{0i} + Bn_b^Q, \quad (6)$$

where m_{0i} ($i = n, p$) represents the baryon mass in vacuum and B the interaction strength.

The quarks are treated as quasifree particles with density-dependent equivalent masses in the framework of equivparticle models [70,73–75], which is described by the Lagrangian density in Eq. (3). Considering the interactions of linear confinement and leading-order perturbation, the quark mass scaling is determined by [70]

$$m_i(n_b) = m_{0i} + \frac{D}{\sqrt[3]{n_b}} + C\sqrt[3]{n_b}, \quad (7)$$

where $m_{0u} = 2.3$ MeV and $m_{0d} = 4.8$ MeV are the current masses of quarks [76]. The parameter D represents the confinement strength, which is related to the chiral restoration density, string tension, and the sum of vacuum chiral condensates. The perturbative strength C is connected to the strong coupling constant. Because of the uncertainties in relevant quantities, the exact values of D and C are still unclear. Nevertheless, it has been estimated that $\sqrt{D}$ approximately lies in the range of 147–270 MeV [75] and $C \lesssim 1.2$ [70].

According to the Typel-Wolter ansatz [51], we adopt density-dependent nucleon-meson coupling constants. For σ and ω mesons, the coupling constants are determined by

$$g_{\phi i}(n_b^B) = g_{\phi i}(n_0)a_\phi \frac{1 + b_\phi(x + d_\phi)^2}{1 + c_\phi(x + e_\phi)^2}, \quad (8)$$

where $\phi = \sigma, \omega$ and $x \equiv n_b^B/n_0$ with n_0 being the saturation density of nuclear matter. a_ϕ, b_ϕ, c_ϕ, d_ϕ, and e_ϕ are five

adjustable parameters describing the density-dependent coupling constants. Meanwhile, a different formula is adopted for the ρ meson, i.e.,

$$g_{\rho i}(n_b^B) = g_{\rho i}(n_0) \exp[-a_\rho(x + b_\rho)]. \quad (9)$$

Based on the Lagrangian density in Eqs. (2)–(4), the meson fields are determined by

$$m_\sigma^2 \sigma = -\sum_{i=n,p} g_{\sigma i} n_i^s, \quad (10)$$

$$m_\omega^2 \omega_0 = \sum_{i=n,p} g_{\omega i} n_i, \quad (11)$$

$$m_\rho^2 \rho_3 = \sum_{i=n,p} g_{\rho i} \tau_{i,3} n_i. \quad (12)$$

Adopting the no-sea approximation, the source currents of fermion i for cold dense matter are given by

$$n_i = \langle \bar{\Psi}_i \gamma^0 \Psi_i \rangle = \frac{g_i \nu_i^3}{6\pi^2}, \quad (13)$$

$$n_i^s = \langle \bar{\Psi}_i \Psi_i \rangle = \frac{g_i (m_i^*)^3}{4\pi^2} \left[x_i \sqrt{x_i^2 + 1} - \operatorname{arcsh}(x_i) \right]. \quad (14)$$

Here we have defined $x_i \equiv \nu_i / m_i^*$ with ν_i being the Fermi momentum and the degeneracy factor g_i taken as $g_{n,p} = 2$, $g_{u,d} = 6$, and $g_{e,\mu} = 2$ for baryons, quarks, and leptons, respectively. The effective mass for baryon b is defined as $m_b^* = m_b(n_b^Q) + g_{\sigma b}\sigma$ with the baryon mass scaling $m_b(n_b^Q)$ indicated in Eq. (6), while for quark q we adopt the mass scaling of Eq. (7), i.e., $m_q^* = m_q(n_b)$. Meanwhile, the masses of leptons remain constant with $m_e^* = 0.511$ MeV and $m_\mu^* = 105.66$ MeV [76]. The single-particle energies of fermions at fixed momentum p are

$$\epsilon_b^B(p) = g_{\omega b}\omega + g_{\rho b}\tau_{b,3}\rho_3 + \Sigma_b^R + \sqrt{p^2 + (m_b^*)^2}, \quad (15)$$

$$\epsilon_q^Q(p) = \Sigma_q^R + \sqrt{p^2 + (m_q^*)^2}, \quad (16)$$

$$\epsilon_l^L(p) = \sqrt{p^2 + (m_l^*)^2}, \quad (17)$$

with the "rearrangement" terms given by

$$\Sigma_b^R = \sum_{i=n,p} \left(\frac{dg_{\sigma i}}{dn_b^B} \sigma n_i^s + \frac{dg_{\omega i}}{dn_b^B} \omega n_i + \frac{dg_{\rho i}}{dn_b^B} \rho_3 \tau_{i,3} n_i \right) + \sum_{i=u,d} \frac{dm_i}{dn_b} n_i^s, \quad (18)$$

TABLE I. Saturation properties of nuclear matter predicted by three different density-dependent covariant density functionals TW99 [51], PKDD [68], and DD-ME2 [69].

	n_0 fm^{-3}	B MeV	K MeV	J MeV	S MeV	L MeV	$K_{\rm sym}$ MeV
TW99	0.153	−16.24	240.2	−540	32.8	55.3	−125
PKDD	0.150	−16.27	262.2	−119	36.8	90.2	−81
DD-ME2	0.152	−16.13	250.8	477	32.3	51.2	−87

$$\Sigma_q^{\rm R} = \frac{1}{3} \sum_{i=n,p,u,d} \frac{{\rm d}m_i}{{\rm d}n_{\rm b}} n_i^s. \tag{19}$$

For quarkyonic matter, the quark-hadron interface in momentum space is set by matching the single-particle energies, i.e.,

$$\epsilon_u^{\rm Q}(\nu_u) + 2\epsilon_d^{\rm Q}(\nu_d) = \epsilon_n^{\rm B}(0),$$
$$2\epsilon_u^{\rm Q}(\nu_u) + \epsilon_d^{\rm Q}(\nu_d) = \epsilon_p^{\rm B}(0), \tag{20}$$

where $\epsilon_i(p_i)$ represents the single-particle energy at a given momentum p_i. In the quarkyonic phase, ν_u and ν_d now represent the maximum momentums for u and d quarks instead of Fermi momentums, above which are baryons and the effects of Pauli blocking exclude the existence of free quarks. The chemical potentials for baryon b and lepton l are then fixed by $\mu_b = \epsilon_b^{\rm B}(\nu_b)$ and $\mu_l = \epsilon_l^{\rm L}(\nu_l)$, respectively. For quarks, we can also define an effective chemical potential $\mu_q = \epsilon_q^{\rm Q}(\nu_q)$, which is nonetheless not the actual one, as ν_q does not correspond to the Fermi surface in the quarkyonic phase.

Finally, the energy density can be determined by

$$E = \sum_i \varepsilon_i(\nu_i, m_i^*) + \sum_{\phi=\sigma,\omega,\rho} \frac{1}{2} m_\phi^2 \phi^2, \tag{21}$$

with the kinetic energy density

$$\begin{aligned} \varepsilon_i(\nu_i, m_i^*) &= \int_0^{\nu_i} \frac{g_i p^2}{2\pi^2} \sqrt{p^2 + (m_i^*)^2}\, dp \\ &= \frac{g_i (m_i^*)^4}{16\pi^2} \left[x_i(2x_i^2+1)\sqrt{x_i^2+1} - {\rm arcsh}(x_i) \right]. \end{aligned} \tag{22}$$

Then the pressure P is obtained with

$$P = \sum_i \mu_i n_i - E. \tag{23}$$

At a given total baryon number density $n_{\rm b}$ and isospin asymmetry

$$\delta \equiv (n_d - n_u + n_n - n_p)/n_{\rm b}, \tag{24}$$

the properties of three types of strongly interacting matter can then be fixed, i.e.,

   (1) Nuclear matter: $n_{\rm b}^{\rm Q} = 0$ with $n_{\rm b} = n_{\rm b}^{\rm B}$.
   (2) Quark matter: $n_{\rm b}^{\rm B} = 0$ with $n_{\rm b} = n_{\rm b}^{\rm Q}$.
   (3) Quarkyonic matter: $n_{\rm b} = n_{\rm b}^{\rm B} + n_{\rm b}^{\rm Q}$ with $n_{\rm b}^{\rm B}$ and $n_{\rm b}^{\rm Q}$ fixed by Eq. (20).

The corresponding mean fields, single-particle energies, and densities are fixed by solving Eqs. (6)–(20) in an iterative manner. Once convergency is reached, the energy density and pressure can then be obtained with Eqs. (21) and (23).

III. RESULTS AND DISCUSSIONS

For baryonic matter described by the Lagrangian density in Eq. (2), we adopt three different density-dependent covariant density functionals TW99 [51], PKDD [68], and DD-ME2 [69]. The corresponding properties of nuclear matter around the saturation density ($n_0 \approx 0.16$ fm^{-3}) are indicated in Table I, which include the binding energy B, incompressibility K, skewness coefficient J, symmetry energy S, slope L, and curvature parameter $K_{\rm sym}$ of nuclear symmetry energy. Note that some of the coefficients are well constrained with $B \approx -16$ MeV, $K = 240 \pm 20$ MeV [77], $S = 31.7 \pm 3.2$ MeV, and $L = 58.7 \pm 28.1$ MeV [78,79], which can be further constrained by considering the recent data from astrophysical observations, heavy-ion collisions, measurements of the neutron skin thicknesses, and nuclear theories [80–84]. The saturation properties of nuclear matter predicted by the covariant density functionals generally coincide with those constraints, except that PKDD predicts slightly larger S and L. In summary, compared with TW99, the functional PKDD predicts larger symmetry energy (S and L), while the energy per baryon for symmetric nuclear matter at suprasaturation densities is significantly increased (larger K and J) if DD-ME2 is adopted.

Based on the aforementioned density functionals, we further consider the possible formation of quarkyonic matter by including explicitly quasifree quarks. The adopted parameter sets $(B, C, \sqrt{D})$ of the baryon and quark mass scalings in Eqs. (6) and (7) are listed in Table II, where B is in MeV/fm^3, C dimensionless, and $\sqrt{D}$ in MeV. To fix the properties of dense stellar matter, leptons fulfilling charge neutrality condition need to be considered, i.e.,

$$\sum_i q_i n_i = 0, \tag{25}$$

where $q_n = 0$, $q_p = 1$, $q_u = 2/3$, $q_d = -1/3$, and $q_e = q_\mu = -1$ are the charge numbers of each particle type. Note that hyperons are not included yet, which will be considered in our future works. Additionally, at fixed total baryon number density $n_{\rm b}$, the number densities of leptons $n_{e,\mu}$, quarks $n_{\rm b}^{\rm Q}$, and isospin asymmetry δ for cold dense stellar matter are fixed by fulfilling the chemical equilibrium condition, i.e.,

TABLE II. The adopted parameter sets $(B, C, \sqrt{D})$ for the baryon and quark mass scalings in Eqs. (6) and (7). The obtained radii $R_{1.4}$ and tidal deformability $\Lambda_{1.4}$ of 1.4-solar-mass compact stars, the maximum mass M_{TOV}, and the maximum sound speed v_{max} of quarkyonic matter are indicated as well.

	B	C	$\sqrt{D}$	$R_{1.4}$	$\Lambda_{1.4}$	M_{TOV}	v_{max}
	MeV/fm^3		MeV	km		$M_\odot$	c
TW99	300	0.7	180	12.27	405	2.04	0.73
	0	0.7	180	12.27	405	1.97	0.67
	300	0.2	180	12.20	386	1.88	0.68
	300	0.7	230	12.27	405	2.08	0.83
PKDD	**150**	**0.7**	**150**	12.80	530	2.06	0.67
	0	0.7	150	12.40	463	2.00	0.67
	150	1.0	150	13.60	751	2.20	0.70
	150	0.7	180	13.63	764	2.20	0.69
DD-ME2	**100**	**0.5**	**160**	12.74	557	2.06	0.65
	300	0.5	160	13.08	666	2.15	0.65
	100	0.7	160	13.17	703	2.19	0.65
	100	0.5	180	13.20	712	2.19	0.63

$$\mu_n - \mu_p = \mu_e = \mu_\mu. \tag{26}$$

The EOSs of neutron star matter are obtained with the energy density E fixed by Eq. (21) and pressure P by Eq. (23).

In Fig. 2, we present the energy per baryon E/n_{b} of nuclear matter and quarkyonic matter in compact stars as functions of the total baryon number density n_{b}. As density

increases, nuclear matter is converted into quarkyonic matter at $n_{\text{b}} \gtrsim 0.1$ fm^{-3}, which becomes more stable as the energy is decreased. The variations of the energy per baryon in quarkyonic matter are far less significant than those of nuclear matter. It is found that the transitions from nuclear matter to quarkyonic matter are mostly second order, except for the case of PKDD adopting the parameter set $B = 0$, $C = 0.7$, and $\sqrt{D} = 150$ MeV, where a first-order quarkyonic transition is identified. The effects of various types of interactions can be examined by varying the corresponding parameters, where the onset densities of quarkyonic transitions and energies of quarkyonic matter increase with the strengths of quark-hadron interaction B, perturbative interaction C, and confinement $\sqrt{D}$. Meanwhile, we note that increasing C leads to a more significant increment in energy at higher densities, which is mainly due to the increasing repulsive interaction described by the quark mass scaling in Eq. (7).

To show more explicitly the variations in the stiffness of the EOSs, we present the velocity of sound v in Fig. 3, which is determined by

$$v = \sqrt{\frac{dP}{dE}}. \tag{27}$$

As the total baryon number density n_{b} increases, the velocity of sound also increases before reaching its peak v_{max} for quarkyonic matter. Such structure in the speed of sound was identified in various previous studies and interpreted as the onset of a new matter state [85–89],

FIG. 2. Energy per baryon E/n_{b} of nuclear matter (solid lines) and quarkyonic matter (dashed lines) as functions of the total baryon number density n_{b}, which are obtained adopting the parameter sets indicated in Table II.
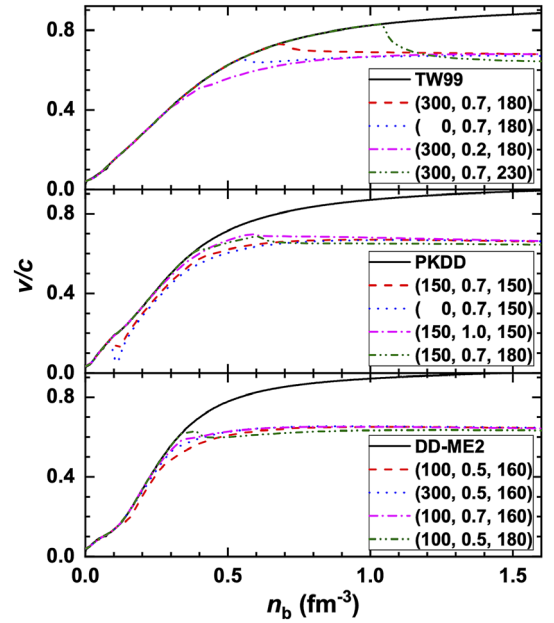
FIG. 3. Velocity of sound v in nuclear matter (solid lines) and quarkyonic matter (dashed lines) obtained with the EOSs presented in Fig. 2.

which corresponds to quarkyonic transition in our current study. At larger densities, the velocity of sound for quarkyonic matter is distinctively smaller than that of nuclear matter, which approaches ~ 0.64 and is slightly larger than the ultrarelativistic limit $1/\sqrt{3}$ (≈ 0.58). Note that, when we take $B = 0$, $C = 0.7$, and $\sqrt{D} = 150$ MeV for PKDD, the quarkyonic transition is of first order and the velocity of sound is zero in the range $n_b \approx 0.1$–0.13 fm^{-3}. Meanwhile, at large enough densities, e.g., $\sim 40 n_0$, perturbative QCD is applicable and we expect the formation of a deconfined quark matter with $v \to 1/\sqrt{3}$ [90–92]. The deviation of v from $1/\sqrt{3}$ is thus attributed to the strong interactions in the quarkyonic phase. Generally speaking, at small densities with the emergence of quarkyonic matter, the velocity of sound increases with B, C, and $\sqrt{D}$, which can be identified as well according to the maximum sound speed $v_{\max}$ indicated in Table II. At larger densities, the velocity of sound increases with C and decreases with $\sqrt{D}$, while varying the quark-hadron interaction strength B has little contribution to v.

Based on the EOSs presented in Fig. 2, the corresponding structures of compact stars are obtained by solving the Tolman-Oppenheimer-Volkov (TOV) equation

$$\frac{dP}{dr} = -\frac{GME}{r^2}\frac{(1+P/E)(1+4\pi r^3 P/M)}{1-2GM/r} \qquad (28)$$

with the subsidiary condition

$$\frac{dM}{dr} = 4\pi E r^2. \qquad (29)$$

The gravity constant is taken as $G = 6.707 \times 10^{-45}$ MeV^{-2}. The dimensionless tidal deformability is calculated by

$$\Lambda = \frac{2k_2}{3}\left(\frac{R}{GM}\right)^5, \qquad (30)$$

where the second Love number k_2 is evaluated by introducing perturbations to the metric [93–95]. Note that a first-order liquid-gas phase transition takes place at subsaturation densities, which forms various types of nonuniform structures, and we have adopted unified neutron star EOSs corresponding to the employed covariant density functionals [96].

In Fig. 4, we present the M-R relations of neutron stars and quarkyonic stars obtained by adopting different combinations of parameters in Table II. The corresponding radius $R_{1.4}$ and tidal deformability $\Lambda_{1.4}$ for $1.4 M_\odot$ stars and the maximum mass M_{TOV} are indicated in Table II as well. Based on various observational data of pulsars, strong constraints on compact star structures are obtained. For example, by analyzing the orbital motion of pulsars in a binary system [97], the masses of PSR J1614-2230 ($1.928 \pm 0.017 M_\odot$) [98] and PSR J0348 + 0432 ($2.01 \pm 0.04 M_\odot$) [99] were measured with high precision. The observation of gravitational waves emitted in the binary neutron star merger event GW170817 has placed strong constraints on the tidal deformability $70 \leq \Lambda_{1.4} \leq 580$, corresponding to a radius of $11.9^{+1.4}_{-1.4}$ km [100]. The simultaneous measurements of masses and radii for PSR J0030 + 0451 and PSR J0740 + 6620 have also placed strong constraints on compact star structures [101–104].

The M-R relation of neutron stars predicted by the covariant density functional TW99 agrees well with the observational constraints [96], while the radii for two-solar-mass neutron stars lie in the lower ends of the PSR J0740 + 6620 constraints [102,104]. Nevertheless, neutron stars obtained with PKDD (larger L) and DD-ME2 (larger J) have larger maximum masses M_{TOV}, radii $R_{1.4}$, and tidal deformabilities $\Lambda_{1.4}$, where $R_{1.4}$ and $\Lambda_{1.4}$ slightly exceed
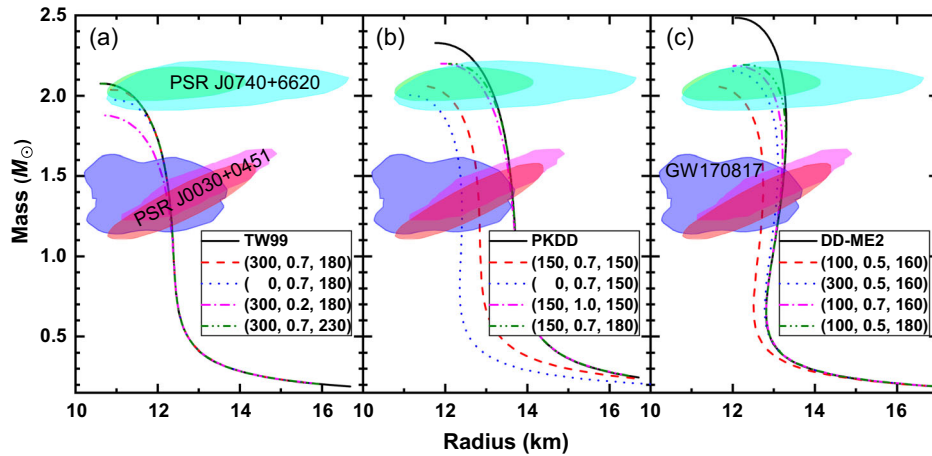
FIG. 4. Mass-radius relations of compact stars obtained with the EOSs presented in Fig. 2. The shaded regions indicate the constraints from the binary neutron star merger event GW170817 within 90% credible region [100], the observational pulse profiles in PSR J0030 + 0451 and PSR J0740 + 6620 within 68% credible region [101–104].
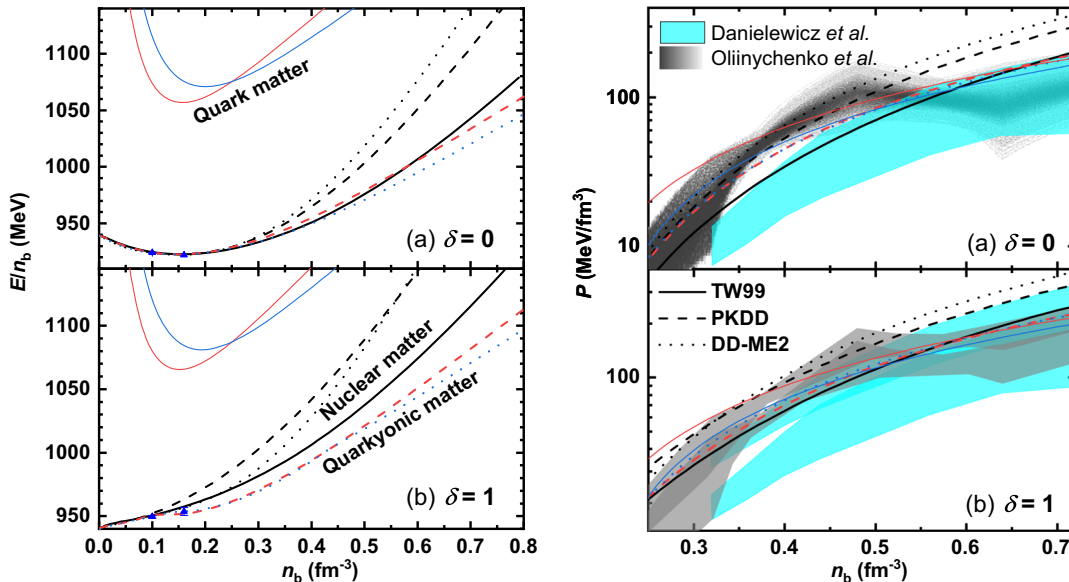
FIG. 5.   Energy per baryon and pressure of nuclear matter (black line), quark matter (color solid line), and quarkyonic matter (color dashed line) with isospin asymmetry (a) $\delta = 0$ and (b) $\delta = 1$. The solid triangles in the left panel indicate the constrains from finite nuclei properties [78,79,105], while the color bands in the right panel correspond to the constraints from the experimental flow data [107,108].

the observational upper limits. With the emergence of quarkyonic matter, the EOSs of quarkyonic matter become softer, and, consequently, quarkyonic stars are more compact with smaller radii and tidal deformabilities. For smaller values of (B, C, $\sqrt{D}$), the EOSs of quarkyonic matter become softer, where M_{TOV}, $R_{1.4}$, and $\Lambda_{1.4}$ decrease. The quarkyonic stars obtained with the parameter sets (100, 0.5, 160) for DD-ME2 and (150, 0.7, 150) and (0, 0.7, 150) for PKDD, thus, become consistent with various constraints from pulsar observations. Note that, for TW99, quarkyonic transition is not favored according to pulsar observations, where quarkyonic matter can emerge only in the center regions of massive stars. Evidently, adopting (300, 0.2, 180) for TW99 predicts a too soft EOS for quarkyonic stars, where the corresponding maximum mass does not reach $2M_{\odot}$ and is, thus, inconsistent with pulsar observations [99]. In such cases, quarkyonic transition is more likely to take place if a large skewness coefficient J or slope of symmetry energy L is confirmed for nuclear matter, e.g., those from PREX-2 [82].

In Fig. 5, we present energy per baryon and pressure of nuclear matter, quark matter, and quarkyonic matter with isospin asymmetry $\delta = 0$ and 1. To fix the properties of quark matter and quarkyonic matter, as indicated by the boldface in Table II, the parameter sets (100, 0.5, 160) for DD-ME2 and (150, 0.7, 150) for PKDD are adopted, which predict quarkyonic stars that are consistent with pulsar observations. Evidently, the deconfined quark matter is highly unstable in comparison with nuclear matter and quarkyonic matter, where the energy per baryon is much larger. The quarkyonic transition takes place at around $1.4n_0$

for symmetric nuclear matter (SNM), while the onset density is decreased significantly for pure neutron matter (PNM) at around $n_{\text{on}} = 0.1$ fm^{-3}. Similar to quarkyonic matter in compact stars, the energy is decreased once quarkyonic transition takes place for both SNM and PNM. The obtained energy per baryon is then compared with the well-constrained nuclear matter properties at n_0 and n_{on}, i.e., $B(n_0) = -16$ MeV, $S(n_0) = 31.7 \pm 3.2$ MeV [78,79], $B(n_{\text{on}}) = -14.1 \pm 0.1$ MeV, and $S(n_{\text{on}}) = 25.5 \pm 1.0$ MeV [105,106]. Evidently, the binding energy of SNM agrees well with the constraints $B(n_{\text{on}}) = -14.1 \pm 0.1$ MeV and $B(n_0) = -16$ MeV. This is not the case for PNM, where PKDD predicts symmetry energy that exceeds the constraint $S(n_0) = 31.7 \pm 3.2$ MeV. The situation is improved if quarkyonic transition takes place for PNM, which well reproduces the constraint on symmetry energy $S(n_0) = 31.7 \pm 3.2$ MeV.

In the right panel in Fig. 5, we compare the pressure of nuclear matter, quark matter, and quarkyonic matter with various constraints from the flow data of heavy-ion collisions [107,108]. Note that there exist many other constraints on the pressure of dense matter [109–113], which are not indicated in Fig. 5, since they generally coincide with those from Refs. [107,108]. For SNM at $n_b \approx 2$–$3n_0$, the pressure obtained by RMF models is generally larger than the constraint provided by Danielewicz et al. [107], which nonetheless coincides with the constraint from Oliinychenko et al. [108]. At larger densities, however, SNM becomes too stiff except for those obtained with the covariant energy density functional TW99. This can be improved if we consider quarkyonic

transitions, where the pressure at $n_b \approx 3$–$5n_0$ coincides with the constraints from the flow data of heavy-ion collisions [107,108]. Similar situations are also observed for PNM, where the pressure obtained with PKDD and DD-ME2 is too large except for TW99 that gives satisfactory results. Note that, at $n_b \approx 2$–$3n_0$, the constraint from Oliinychenko *et al.* [108] gives a larger upper limit on pressure as well, which supports the predictions of RMF models. At larger densities, it is necessary to consider quarkyonic transitions if the covariant density functionals PKDD and DD-ME2 are adopted, where the pressure of PNM is decreased so that it is consistent with the constraints from heavy-ion collisions [107].

IV. CONCLUSION

In this work, by combining RMF models and equivparticle models with density-dependent quark masses [66], we extend RMF models to include quark degrees of freedom, where we have constructed explicitly a quark Fermi sea and a baryonic Fermi surface to model the quarkyonic phase. In contrast to previous treatments of simply removing lower-momentum components [39–42], baryons with momentums ranging from zero to Fermi momentums are included in our approach, which are more reasonable in analogy to the formation of Cooper pairs that are dominated by zero momentum components. The nuclear matter, quark matter, and quarkyonic matter are treated in a unified manner. As we increase the density of nuclear matter, quarkyonic matter emerges and the energy per baryon decreases; i.e., quarkyonic matter is more stable than nuclear matter or quark matter, and energy minimization is still applicable to obtain the microscopic properties of quarkyonic matter.

We have adopted three different effective baryon-baryon interactions TW99 [51], PKDD [68], and DD-ME2 [69], which indicate different saturation properties for nuclear matter with a larger slope of symmetry energy L for PKDD

and larger skewness coefficient J for DD-ME2 in comparison with TW99. Note that the covariant density functional TW99 gives satisfactory predictions for the nuclear matter properties in both neutron stars and heavy-ion collisions, where the quarkyonic transition is unfavorable according to both experimental and astrophysical constraints. This is not the case for either PKDD or DD-ME2, which predict too stiff EOSs for nuclear matter in neutron stars and heavy-ion collisions. The radii and tidal deformabilities of neutron stars are too large with $R_{1.4} = 13.63$ km and $\Lambda_{1.4} = 764$ for PKDD and $R_{1.4} = 13.2$ km and $\Lambda_{1.4} = 712$ for DD-ME2, which exceed the constraints $70 \leq \Lambda_{1.4} \leq 580$ from the binary neutron star merger event GW170817 [100] and the radius measurements of PSR J0030 + 0451 with $R_{1.4} = 12.45 \pm 0.65$ km [104]. Meanwhile, the functionals PKDD and DD-ME2 predict too large pressure for nuclear matter at $n_b \approx 3$–$5n_0$ according to the constraints from the flow data of heavy-ion collisions [107,108]. This situation can be improved if quarkyonic transition takes place, where the EOSs become softer and can accommodate various experimental and astrophysical constraints.

[1] K. Fukushima, C. Kouvaris, and K. Rajagopal, Phys. Rev. D **71**, 034002 (2005).

[2] D. Voskresensky, Prog. Part. Nucl. Phys. **130**, 104030 (2023).

[3] V. A. Dexheimer and S. Schramm, Phys. Rev. C **81**, 045201 (2010).

[4] H. Heiselberg, C. J. Pethick, and E. F. Staubo, Phys. Rev. Lett. **70**, 1355 (1993).

[5] N. K. Glendenning, Phys. Rep. **342**, 393 (2001).

[6] D. Voskresensky, M. Yasuhira, and T. Tatsumi, Phys. Lett. B **541**, 93 (2002).

[7] T. Tatsumi, M. Yasuhira, and D. Voskresensky, Nucl. Phys. **A718**, 359 (2003).

[8] D. Voskresensky, M. Yasuhira, and T. Tatsumi, Nucl. Phys. **A723**, 291 (2003).

[9] T. Endo, T. Maruyama, S. Chiba, and T. Tatsumi, Nucl. Phys. **A749**, 333 (2005).

[10] T. Maruyama, S. Chiba, H.-J. Schulze, and T. Tatsumi, Phys. Rev. D **76**, 123015 (2007).

[11] G. X. Peng, A. Li, and U. Lombardo, Phys. Rev. C **77**, 065807 (2008).

[12] N. Yasutake, R. Łastowiecki, S. Benić, D. Blaschke, T. Maruyama, and T. Tatsumi, Phys. Rev. C **89**, 065803 (2014).

[13] C.-J. Xia, T. Maruyama, N. Yasutake, and T. Tatsumi, Phys. Rev. D **99**, 103017 (2019).

[14] K. Maslov, N. Yasutake, D. Blaschke, A. Ayriyan, H. Grigorian, T. Maruyama, T. Tatsumi, and D. N. Voskresensky, Phys. Rev. C **100**, 025802 (2019).

[15] C.-J. Xia, T. Maruyama, N. Yasutake, T. Tatsumi, H. Shen, and H. Togashi, Phys. Rev. D **102**, 023031 (2020).

[16] S. Borsanyi, Z. Fodor, C. Hoelbling, S. D. Katz, S. Krieg, and K. K. Szabo, Phys. Lett. B **730**, 99 (2014).

[17] A. Bazavov *et al.* (HotQCD Collaboration), Phys. Rev. D **90**, 094503 (2014).

[18] G. Baym, Physica (Amsterdam) **96A**, 131 (1979).

[19] T. Çelik, F. Karsch, and H. Satz, Phys. Lett. **97B**, 128 (1980).

[20] T. Schäfer and F. Wilczek, Phys. Rev. Lett. **82**, 3956 (1999).

[21] K. Fukushima, Phys. Lett. B **591**, 277 (2004).

[22] T. Hatsuda, M. Tachibana, N. Yamamoto, and G. Baym, Phys. Rev. Lett. **97**, 122001 (2006).

[23] K. Maeda, G. Baym, and T. Hatsuda, Phys. Rev. Lett. **103**, 085301 (2009).

[24] K. Masuda, T. Hatsuda, and T. Takatsuka, Astrophys. J. **764**, 12 (2013).

[25] K. Masuda, T. Hatsuda, and T. Takatsuka, Prog. Theor. Exp. Phys. **2013**, 073D01 (2013).

[26] T. Zhao, S.-S. Xu, Y. Yan, X.-L. Luo, X.-J. Liu, and H.-S. Zong, Phys. Rev. D **92**, 054012 (2015).

[27] T. Kojo, P. D. Powell, Y. Song, and G. Baym, Phys. Rev. D **91**, 045003 (2015).

[28] K. Masuda, T. Hatsuda, and T. Takatsuka, Eur. Phys. J. A **52**, 65 (2016).

[29] D. L. Whittenbury, H. H. Matevosyan, and A. W. Thomas, Phys. Rev. C **93**, 035807 (2016).

[30] Z. Bai, H. Chen, and Y.-x. Liu, Phys. Rev. D **97**, 023018 (2018).

[31] G. Baym, S. Furusawa, T. Hatsuda, T. Kojo, and H. Togashi, Astrophys. J. **885**, 42 (2019).

[32] Y.-J. Huang, L. Baiotti, T. Kojo, K. Takami, H. Sotani, H. Togashi, T. Hatsuda, S. Nagataki, and Y.-Z. Fan, Phys. Rev. Lett. **129**, 181101 (2022).

[33] Y. Fujimoto, K. Fukushima, K. Hotokezaka, and K. Kyutoku, Phys. Rev. Lett. **130**, 091404 (2023).

[34] K. Fukushima and T. Kojo, Astrophys. J. **817**, 180 (2016).

[35] K. Hebeler, J. M. Lattimer, C. J. Pethick, and A. Schwenk, Phys. Rev. Lett. **105**, 161102 (2010).

[36] L. McLerran, Nucl. Phys. **A830**, 709c (2009).

[37] L. McLerran and R. D. Pisarski, Nucl. Phys. **A796**, 83 (2007).

[38] L. McLerran, K. Redlich, and C. Sasaki, Nucl. Phys. **A824**, 86 (2009).

[39] L. McLerran and S. Reddy, Phys. Rev. Lett. **122**, 122701 (2019).

[40] J. Margueron, H. Hansen, P. Proust, and G. Chanfray, Phys. Rev. C **104**, 055803 (2021).

[41] G. Cao and J. Liao, J. High Energy Phys. 10 (2020) 168.

[42] G. Cao, Phys. Rev. D **105**, 114020 (2022).

[43] A. Park, K. S. Jeong, and S. H. Lee, Phys. Rev. D **104**, 094024 (2021).

[44] A. Park and S. H. Lee, Phys. Rev. D **105**, 114034 (2022).

[45] *Relativistic Density Functional for Nuclear Structure*, International Review of Nuclear Physics Vol. 10, edited by J. Meng (World Scientific, Singapore, 2016).

[46] P.-G. Reinhard, Rep. Prog. Phys. **52**, 439 (1989).

[47] P. Ring, Prog. Part. Nucl. Phys. **37**, 193 (1996).

[48] J. Meng, H. Toki, S. Zhou, S. Zhang, W. Long, and L. Geng, Prog. Part. Nucl. Phys. **57**, 470 (2006).

[49] N. Paar, D. Vretenar, E. Khan, and G. Colò, Rep. Prog. Phys. **70**, R02 (2007).

[50] J. Meng and S. G. Zhou, J. Phys. G **42**, 093101 (2015).

[51] S. Typel and H. Wolter, Nucl. Phys. **A656**, 331 (1999).

[52] D. Vretenar, W. Pöschl, G. A. Lalazissis, and P. Ring, Phys. Rev. C **57**, R1060 (1998).

[53] B.-N. Lu, E.-G. Zhao, and S.-G. Zhou, Phys. Rev. C **84**, 014328 (2011).

[54] X. Roca-Maza, X. Viñas, M. Centelles, P. Ring, and P. Schuck, Phys. Rev. C **84**, 054309 (2011).

[55] R. Belvedere, D. Pugliese, J. A. Rueda, R. Ruffini, and S.-S. Xue, Nucl. Phys. **A883**, 1 (2012).

[56] C. Chen, Q.-K. Sun, Y.-X. Li, and T.-T. Sun, Sci. China Phys. Mech. Astron. **64**, 282011 (2021).

[57] N. Glendenning, *Compact Stars. Nuclear Physics, Particle Physics, and General Relativity* (Springer-Verlag, Berlin, 2000), 2nd ed., ISBN 978-0-387-98977-8.

[58] S. F. Ban, J. Li, S. Q. Zhang, H. Y. Jia, J. P. Sang, and J. Meng, Phys. Rev. C **69**, 045805 (2004).

[59] F. Weber, R. Negreiros, P. Rosenfield, and M. Stejner, Prog. Part. Nucl. Phys. **59**, 94 (2007).

[60] W. H. Long, B. Y. Sun, K. Hagino, and H. Sagawa, Phys. Rev. C **85**, 025806 (2012).

[61] T. T. Sun, B. Y. Sun, and J. Meng, Phys. Rev. C **86**, 014305 (2012).

[62] S. Wang, H. F. Zhang, and J. M. Dong, Phys. Rev. C **90**, 055801 (2014).

[63] A. Fedoseew and H. Lenske, Phys. Rev. C **91**, 034307 (2015).

[64] Z.-F. Gao, N. Wang, H. Shan, X.-D. Li, and W. Wang, Astrophys. J. **849**, 19 (2017).

[65] T.-T. Sun, C.-J. Xia, S.-S. Zhang, and M. S. Smith, Chin. Phys. C **42**, 025101 (2018).

[66] C.-J. Xia, S.-S. Xue, and S.-G. Zhou, Nuclear matter, quarkyonic matter, and phase transitions in hybrid stars, in *Proceedings of the Workshop on Quarks and Compact Stars 2017 (QCS2017)* (2018), 10.7566/JPSCP.20.011010.

[67] T. Kojo, D. Hou, J. Okafor, and H. Togashi, Phys. Rev. D **104**, 063036 (2021).

[68] W.-H. Long, J. Meng, N. V. Giai, and S.-G. Zhou, Phys. Rev. C **69**, 034319 (2004).

[69] G. A. Lalazissis, T. Nikšić, D. Vretenar, and P. Ring, Phys. Rev. C **71**, 024312 (2005).

[70] C. J. Xia, G. X. Peng, S. W. Chen, Z. Y. Lu, and J. F. Xu, Phys. Rev. D **89**, 105027 (2014).

[71] G. Röpke, P. Schuck, Y. Funaki, H. Horiuchi, Z. Ren, A. Tohsaki, C. Xu, T. Yamada, and B. Zhou, Phys. Rev. C **90**, 034304 (2014).

[72] C. Xu, Z. Ren, G. Röpke, P. Schuck, Y. Funaki, H. Horiuchi, A. Tohsaki, T. Yamada, and B. Zhou, Phys. Rev. C **93**, 011306 (2016).

[73] G. X. Peng, H. C. Chiang, J. J. Yang, L. Li, and B. Liu, Phys. Rev. C **61**, 015201 (1999).

[74] G. X. Peng, U. Lombardo, M. Loewe, and H. C. Chiang, Phys. Lett. B **548**, 189 (2002).

[75] X. J. Wen, X. H. Zhong, G. X. Peng, P. N. Shen, and P. Z. Ning, Phys. Rev. C **72**, 015204 (2005).

[76] Particle Data Group, Chin. Phys. C **38**, 090001 (2014).

[77] S. Shlomo, V. M. Kolomietz, and G. Colò, Eur. Phys. J. A **30**, 23 (2006).

[78] B.-A. Li and X. Han, Phys. Lett. B **727**, 276 (2013).

[79] M. Oertel, M. Hempel, T. Klähn, and S. Typel, Rev. Mod. Phys. **89**, 015007 (2017).

[80] Y. Zhang, M. Liu, C.-J. Xia, Z. Li, and S. K. Biswal, Phys. Rev. C **101**, 034303 (2020).

[81] W.-J. Xie and B.-A. Li, J. Phys. G **48**, 025110 (2021).

[82] PREX Collaboration, Phys. Rev. Lett. **126**, 172502 (2021).

[83] R. Essick, I. Tews, P. Landry, and A. Schwenk, Phys. Rev. Lett. **127**, 192701 (2021).

[84] CREX Collaboration, Phys. Rev. Lett. **129**, 042501 (2022).

[85] E. Annala, T. Gorda, A. Kurkela, J. Nättilä, and A. Vuorinen, Nat. Phys. **16**, 907 (2020).

[86] Y.-L. Ma and M. Rho, Prog. Part. Nucl. Phys. **113**, 103791 (2020).

[87] H.-M. Jin, C.-J. Xia, T.-T. Sun, and G.-X. Peng, Phys. Lett. B **829**, 137121 (2022).

[88] H. Tan, V. Dexheimer, J. Noronha-Hostler, and N. Yunes, Phys. Rev. Lett. **128**, 161101 (2022).

[89] M.-Z. Han, Y.-J. Huang, S.-P. Tang, and Y.-Z. Fan, Sci. Bull. **68**, 913 (2023).

[90] B. A. Freedman and L. D. McLerran, Phys. Rev. D **16**, 1169 (1977).

[91] E. S. Fraga and P. Romatschke, Phys. Rev. D **71**, 105014 (2005).

[92] A. Kurkela, P. Romatschke, and A. Vuorinen, Phys. Rev. D **81**, 105021 (2010).

[93] T. Damour and A. Nagar, Phys. Rev. D **80**, 084035 (2009).

[94] T. Hinderer, B. D. Lackey, R. N. Lang, and J. S. Read, Phys. Rev. D **81**, 123016 (2010).

[95] S. Postnikov, M. Prakash, and J. M. Lattimer, Phys. Rev. D **82**, 024016 (2010).

[96] C.-J. Xia, T. Maruyama, A. Li, B. Y. Sun, W.-H. Long, and Y.-X. Zhang, Commun. Theor. Phys. **74**, 095303 (2022).

[97] J. M. Lattimer, Annu. Rev. Nucl. Part. Sci. **62**, 485 (2012).

[98] E. Fonseca *et al.*, Astrophys. J. **832**, 167 (2016).

[99] J. Antoniadis *et al.*, Science **340**, 1233232 (2013).

[100] LIGO Scientific and Virgo Collaborations, Phys. Rev. Lett. **121**, 161101 (2018).

[101] T. E. Riley, A. L. Watts, S. Bogdanov, P. S. Ray, R. M. Ludlam, S. Guillot, Z. Arzoumanian, C. L. Baker, A. V. Bilous, D. Chakrabarty, K. C. Gendreau, A. K. Harding, W. C. G. Ho, J. M. Lattimer, S. M. Morsink, and T. E. Strohmayer, Astrophys. J. **887**, L21 (2019).

[102] T. E. Riley *et al.*, Astrophys. J. **918**, L27 (2021).

[103] M. C. Miller *et al.*, Astrophys. J. **887**, L24 (2019).

[104] M. C. Miller *et al.*, Astrophys. J. **918**, L28 (2021).

[105] B. A. Brown, Phys. Rev. Lett. **111**, 232502 (2013).

[106] M. Centelles, X. Roca-Maza, X. Viñas, and M. Warda, Phys. Rev. Lett. **102**, 122502 (2009).

[107] P. Danielewicz, R. Lacey, and W. G. Lynch, Science **298**, 1592 (2002).

[108] D. Oliinychenko, A. Sorensen, V. Koch, and L. McLerran, arXiv:2208.11996.

[109] C. Fuchs, Prog. Part. Nucl. Phys. **53**, 113 (2004).

[110] W. Lynch, M. Tsang, Y. Zhang, P. Danielewicz, M. Famiano, Z. Li, and A. Steiner, Prog. Part. Nucl. Phys. **62**, 427 (2009).

[111] A. Le Fèvre, Y. Leifels, W. Reisdorf, J. Aichelin, and C. Hartnack, Nucl. Phys. **A945**, 112 (2016).

[112] T. Malik, M. Ferreira, B. K. Agrawal, and C. Providência, Astrophys. J. **930**, 17 (2022).

[113] N. K. Patra, S. M. A. Imam, B. K. Agrawal, A. Mukherjee, and T. Malik, Phys. Rev. D **106**, 043024 (2022).